"Combination of insolation and ice-sheet forcing drive enhanced humidity in northern subtropical regions during MIS 13"

Oliveira D. ; Desprat S. ; Yin, Qiuzhen ; Rodrigues T. ; Naughton F. ; Trigo R. ; Su, Qianqian ; Grimalt J.O. ; Alonso-Garciah M. ; Voelker A.H.L. ; Abrantes F. ; Sánchez Goñi F.M.

ABSTRACT

Marine Isotope Stage (MIS) 13, ~533-478 ka, has received particular attention due to the unexpected enhancement of monsoon systems under a cool climate characterized by lower atmospheric CO2 and larger ice volume than many other interglacials. Key questions remain about its regional expression (intensity, climate variability, length), and underlying forcing factors, in particular at the mid-latitudes. Here we examine the SW Iberian vegetation, terrestrial climate and sea surface temperature (SST) variability during MIS 13 by combining pollen and biomarker data from IODP Site U1385 with climatemodel experiments. We show, for the first time, that despite strong precessional forcing, MIS 13 stands out for its large forest expansions with a reduced Mediterranean character alternating with muted forest contractions, indicating that this stage is marked by a cool-temperate climate regime with high levels of humidity. Results of our data-model comparison reveal that MIS 13 orbitally driven SW Iberian climate and vegetation changes are modulated by the relatively strong ice-sheet forcing. We find that the Northern Hemisphere ice-sheets prescribed at the MIS 13 climate optimum reinforce the insolation effect by increasing the tree fraction and both winter and summer precipitation. We propose that the interactions between ice-sheets and major atmospheric circulation systems may have resulted in the persistent influence of the mid-latitude cells over the SW Iberian region, which led to intensified moisture availability and reduced seasonality, and, in turn, to a pronounced expansion...

CITE THIS VERSION

Oliveira D. ; Desprat S. ; Yin, Qiuzhen ; Rodrigues T. ; Naughton F. ; et. al. *Combination of insolation and ice-sheet forcing drive enhanced humidity in northern subtropical regions during MIS 13.* In: *Quaternary Science Reviews*, Vol. 247, p. 106573 (2020) http://hdl.handle.net/2078.1/238101 -- DOI : 10.1016/j.quascirev.2020.106573

Quaternary Science Reviews 247 (2020) 106573

Contents lists available at ScienceDirect

Quaternary Science Reviews

journal homepage: www.elsevier.com/locate/quascirev

Combination of insolation and ice-sheet forcing drive enhanced humidity in northern subtropical regions during MIS 13

Dulce Oliveira [a, b, *], Stéphanie Desprat [c, d], Qiuzhen Yin [e], Teresa Rodrigues [a, b], Filipa Naughton [a, b], Ricardo M. Trigo [f], Qianqian Su [e], Joan O. Grimalt [g], Montserrat Alonso-Garcia [h, a], Antje H.L. Voelker [a, b], Fátima Abrantes [a, b], Maria Fernanda Sánchez Goñi [c, d]

[a] *CCMAR, Centro de Ciências do Mar, Universidade do Algarve, Campus de Gambelas, 8005-139, Faro, Portugal*
[b] *Divisão de Geologia e Georecursos Marinhos, Instituto Português do Mar e da Atmosfera (IPMA), Av. Doutor Alfredo Magalhães Ramalho 6, 1495-165, Algés, Portugal*
[c] *Ecole Pratique des Hautes Etudes (EPHE, PSL University), F-33615, Pessac, France*
[d] *Université Bordeaux, EPOC, UMR 5805, F-33615, Pessac, France*
[e] *Georges Lemaître Center for Earth and Climate Research, Earth and Life Institute, Université catholique de Louvain, Louvain-la-Neuve, Belgium*
[f] *Instituto Dom Luiz, Universidade de Lisboa, 1749-016, Lisboa, Portugal*
[g] *Department of Environmental Chemistry, Institute of Environmental Assessment and Water Research (IDAEA), Spanish Council for Scientific Research (CSIC), 08034, Barcelona, Spain*
[h] *Department of Geology- Paleontology, University of Salamanca, Pza. de los Caídos, 37008, Salamanca, Spain*

A R T I C L E I N F O

Article history:
Received 20 May 2020
Received in revised form
13 August 2020
Accepted 29 August 2020
Available online xxx

Keywords:
Mid-Brunhes event
Interglacial MIS 13
Mediterranean vegetation
Model-data comparison
Insolation
Ice-sheets

A B S T R A C T

Marine Isotope Stage (MIS) 13, ~533–478 ka, has received particular attention due to the unexpected enhancement of monsoon systems under a cool climate characterized by lower atmospheric CO_2 and larger ice volume than many other interglacials. Key questions remain about its regional expression (intensity, climate variability, length), and underlying forcing factors, in particular at the mid-latitudes. Here we examine the SW Iberian vegetation, terrestrial climate and sea surface temperature (SST) variability during MIS 13 by combining pollen and biomarker data from IODP Site U1385 with climate-model experiments. We show, for the first time, that despite strong precessional forcing, MIS 13 stands out for its large forest expansions with a reduced Mediterranean character alternating with muted forest contractions, indicating that this stage is marked by a cool-temperate climate regime with high levels of humidity. Results of our data-model comparison reveal that MIS 13 orbitally driven SW Iberian climate and vegetation changes are modulated by the relatively strong ice-sheet forcing. We find that the Northern Hemisphere ice-sheets prescribed at the MIS 13 climate optimum reinforce the insolation effect by increasing the tree fraction and both winter and summer precipitation. We propose that the interactions between ice-sheets and major atmospheric circulation systems may have resulted in the persistent influence of the mid-latitude cells over the SW Iberian region, which led to intensified moisture availability and reduced seasonality, and, in turn, to a pronounced expansion of the temperate forest.

1. Introduction

The Mid-Brunhes Event (MBE) represents an important climate transition occurring between MIS 12 and MIS 11 at ~430 ka (Jansen et al., 1986). Interglacial periods before this transition (MIS 13, 15, 17 and 19) appear in general to be longer and characterized by larger ice-sheets, lower sea-level, cooler temperatures in Antarctica and lower greenhouse gases (GHG) concentrations than the more recent ones (MIS 5, 7, 9 and 11) (e.g., Lisiecki and Raymo, 2005; Jouzel et al., 2007; Lüthi et al., 2008; Elderfield et al., 2012). However, the dissimilarities between individual interglacials in terms of

* Corresponding author. Centro de Ciências do Mar, Universidade do Algarve, Campus de Gambelas, 8005-139, Faro, Portugal.
E-mail addresses: dulce.oliveira@ipma.pt, dulce_oliveiraa@hotmail.com (D. Oliveira).

https://doi.org/10.1016/j.quascirev.2020.106573

their structure, intensity and climate forcings before and after the MBE transition are not yet fully understood mainly due to the scarcity of detailed and long paleoclimate records, especially from terrestrial environments (Lang and Wolff, 2011; Yin and Berger, 2010, 2012; Candy and McClymont, 2013; Past Interglacials Working Group of PAGES, 2016). Marine Isotope Stage (MIS) 13 (533–478 ka; Lisiecki and Raymo, 2005) is a pre-MBE interglacial of particular interest as it stands out for its complex and unusual climate signature. This long interglacial has been considered as the weakest, coolest and most glaciated interglacial of the past 800 kyr globally, despite regional exceptions (e.g., Guo et al., 2009; Lang and Wolff, 2011; Candy et al., 2015; Past Interglacials Working Group of PAGES, 2016; de Vernal and Hillaire-Marcel, 2008; Cortina et al., 2016). Unexpectedly, it is associated with a remarkably strong East Asian summer monsoon (EASM), representing the wettest period of the past 800 kyr on the Chinese Loess Plateau (e.g., Yin and Guo, 2008; Guo et al., 2009; Lu et al., 2020), and also with intense monsoons in Africa and India (e.g., Bassinot et al., 1994; Rossignol-Strick et al., 1998). The occurrence of such enhanced monsoons during a cool and glaciated interglacial characterized by relatively low CO_2, CH_4 and not atypical incoming insolation compared to other interglacials, has been pointed out as a “seeming climate paradox” (Yin and Guo, 2008). Although there is still some debate about the driving mechanisms of this “seeming paradox” (Yin and Guo, 2008), recent modeling experiments have shown that a strong EASM could result from a combination of insolation and ice-sheet forcing, with the Eurasian ice-sheet playing a crucial role in reinforcing the monsoon precipitation (Yin et al., 2008, 2009; Muri et al., 2012, 2013; Sundaram et al., 2012). MIS 13 is also characterized by the most prominent global benthic carbon isotope excursion ($\delta^{13}C_b$) of the last 800 kyr despite relatively low levels of atmospheric CO_2 and global ocean export productivity (e.g., Raymo et al., 1990; Wang et al., 2004; Barth et al., 2018). Such outstanding $\delta^{13}C_b$ enrichment can also result from a change in the carbon reservoir rather than ocean circulation. A higher monsoon precipitation would have increased the forested areas in these regions of the Northern Hemisphere (NH), enabling a higher storage of light carbon in the terrestrial reservoir (Barth et al., 2018). Notwithstanding the clear evidence for strong precipitation and consequent increase in the terrestrial biomass in the monsoon regions during MIS 13 (e.g., Yin and Guo, 2008; Yin et al., 2008), due to the paucity of studies, key questions remain concerning the distribution of the forest in other important areas of the NH, such as southern Europe. So far, the expression of MIS 13 in this region is only documented by discontinuous continental records with strong local character and/or uncertain chronology (Russo Ermolli et al., 2015; Margari et al., 2018 and references therein; Di Rita and Sottili, 2019) and long lacustrine pollen sequences with a relatively low temporal resolution over MIS 13 (Tenaghi Philippon, Greece: Tzedakis et al., 2006; and Lake Ohrid, Balkan Peninsula; Wagner et al., 2019). Therefore, deciphering controlling factors of interglacial forest development and regional climate is critical. Model simulations using the LOVECLIM model suggest that insolation is the main driver for tree cover changes during interglacial periods in sub-tropical regions (Yin and Berger, 2012). These simulations do not include ice volume changes, although other recent modeling research shows that both ice-sheet size and configuration also play an important role (Bouttes et al., 2018).

Here we document the southwestern European vegetation and climate dynamics during MIS 13 at unprecedented time resolution (centennial-scale) from a multiproxy study of the SW Iberian margin Integrated Ocean Drilling Program (IODP) Site U1385, which allows a direct comparison between terrestrial and marine climatic indicators, and therefore, the reconstruction of vegetation-based regional atmospheric conditions and their relationships with oceanic temperature variability and ice volume changes. To assess the impacts of insolation, GHG and ice-sheets on the regional vegetation and climate at the interglacial optimum we also performed a suite of experiments with the LOVECLIM Earth system model (Brovkin et al., 1997).

2. Regional setting

The deep-sea Site U1385 or “Shackleton Site” (37°34.285′N, 10°7.562′W; 2578 m below sea-level), drilled on the SW Iberian margin, is under the influence of the surface Portugal Current System, the southern branch of the eastern subtropical gyre (Fig. 1). This system is composed by two major currents, the Iberian Poleward and Portugal Currents, which are mainly controlled by the strength and direction of the offshore winds (e.g., Fiúza, 1984; Teles-Machado et al., 2016). During winter, the SW Iberian region is strongly affected by the North Atlantic westerlies and associated jet stream, whereas during the summer the influence of the northward expansion of the Azores high-pressure system prevails and strong northerly winds induce coastal upwelling (Trigo et al., 2004; Lionello et al., 2006). These atmospheric circulation patterns result in a Mediterranean climate characterized by high seasonal contrast (mild-rainy winters and dry-warm summers) that enables the development of Mediterranean vegetation dominated by conifers (*Pinus*, *Juniperus*) at the highest elevations and deciduous oak at the mid-altitudes. Evergreen oak and Mediterranean sclerophylls (*Olea sylvestris*, *Pistacia lentiscus*, *Phillyrea*) are widespread at lower altitudes in warmer zones (Blanco Castro et al., 1997). Shrub communities mainly composed of heathlands (Ericaceae) dominate the zones with relatively high humidity, while rockroses (Cistaceae) occupy drier environments. As shown by the studies of Naughton et al. (2007) and Morales-Molino et al. (2020), the marine pollen signature from the western Iberian margin provides a reliable integrated image of the vegetation of the adjacent continent because the fluvial systems of the Tejo and Sado rivers are the main pollen suppliers to offshore deep-sea sediments.

3. Material and methods

3.1. Chronological framework

The reference chronological framework provided by Hodell et al. (2015) for Site U1385 encompasses four depth-age models derived from oxygen isotope stratigraphy, orbital tuning and correlation to other reference records. Here we use a revised version of the LR04-derived chronology that extends back to ~1.45 Myr with a mean sedimentation rate of 10.9 cm/kyr. This chronology was developed by correlating the low-resolution (20 cm) benthic oxygen isotope ($\delta^{18}O_b$) record of Site U1385 to the LR04 global $\delta^{18}O_b$ stack of Lisiecki and Raymo (2005). To better constrain the MIS 13 stratigraphy, we identified two additional age-depth tie points, the MIS 13a $\delta^{18}O_b$ peak at ~401 ka and the MIS 13-12 transition at 478 ka (Lisiecki and Raymo, 2005) (Table 1). Age-depth modeling was based on linear interpolation between the seven age control points from ~469 to 540 ka (Table 1). High sedimentation rates and sampling resolution (<4 cm) provide the highest temporal resolution available for Southern European pollen and sea surface temperature (SST) records spanning the entire MIS 13, with a mean resolution of ~253 yr and ~167 yr, respectively.

Multiple deep-sea $\delta^{18}O_b$ records show that MIS 13 is characterized by a first substage, MIS 13c encompassing the light isotopic event MIS 13.3, followed by substage MIS 13b containing the heavy isotopic event 13.2. The third substage MIS 13a, which is generally considered as the full interglacial (Past Interglacials Working Group of PAGES, 2016), incorporates the two light isotopic events 13.13

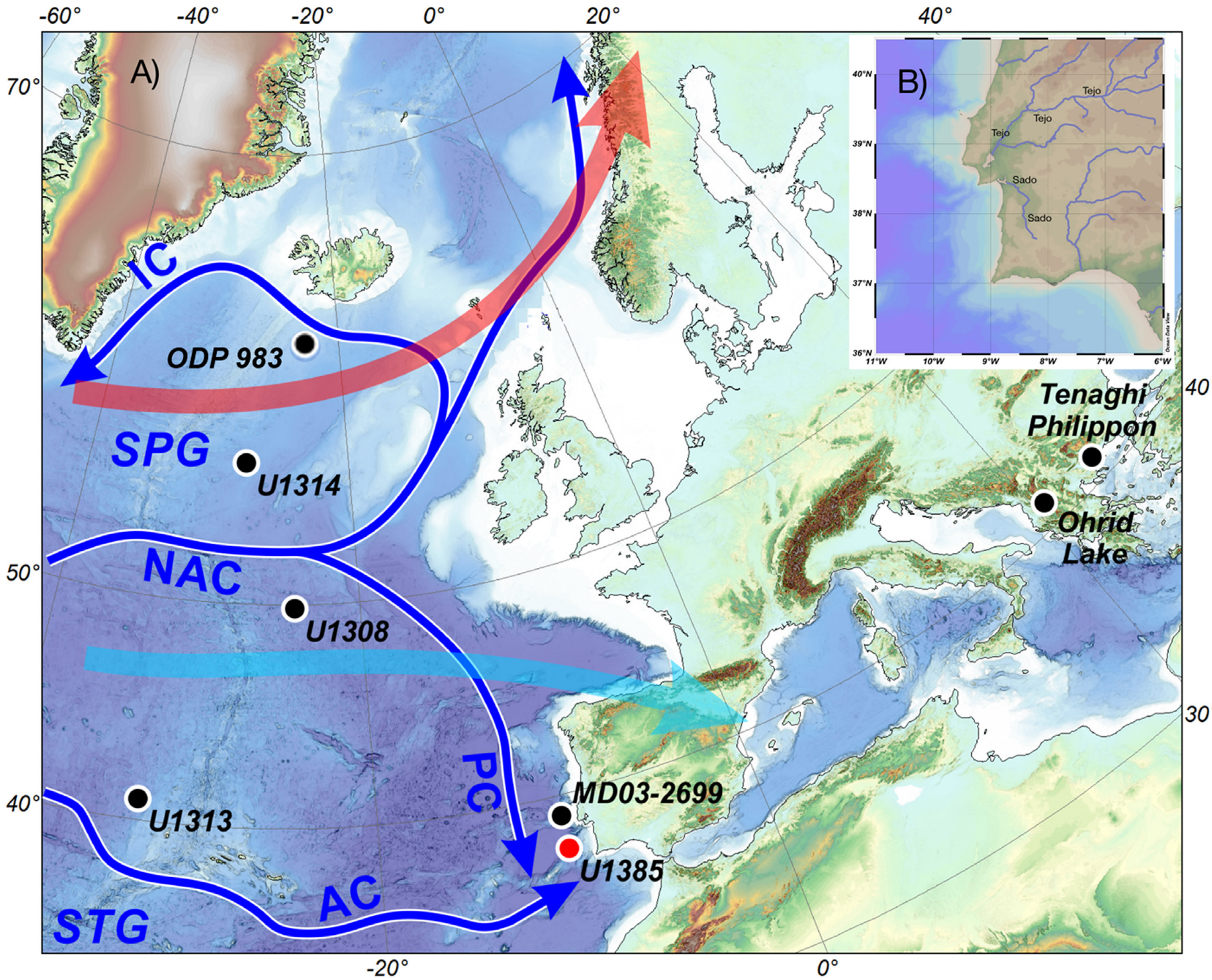

Fig. 1. A) Location of IODP Site U1385 and European and North Atlantic records referred to in this study: ODP Site 983 (Barker et al., 2019); Site U1314 (Alonso-Garcia et al., 2011); Site U1308 (Hodell et al., 2008); MD03-2699 (Voelker et al., 2010; Rodrigues et al., 2011); Site U1313 (Naafs et al., 2012); Tenaghi Philippon (Tzedakis et al., 2006); Lake Ohrid (Wagner et al., 2019). Blue arrows represent the superficial water circulation: NAC: North Atlantic Current, IC: Irminger Current, PC: Portugal Current, AC: Azores Current, SPG and STG: Polar and Subtropical Gyre. The meridional and zonal trajectory of the atmospheric westerlies is shown in red and blue arrows, respectively. B) Location of Tejo and Sado river basins. (For interpretation of the references to color in this figure legend, the reader is referred to the Web version of this article.)

Table 1
Site U1385 age-depth tie points and sedimentation rates. crmcd: corrected revised meter composite depth. *New control points added for this study.

Site U1385 Depth (crmcd)	Control points LR04 Age (ka)	Sed. Rate (cm/kyr)
56.35	446.99	
58.40*	478.00*	6.61
60.85*	491.01*	18.83
62.82	502.10	17.76
66.73	527.19	15.57
67.93	533.93	17.83
73.34	583.43	10.93

and 13.11 (double peak), separated by the heavy isotopic event 13.12 (e.g., Bassinot et al., 1994; Lisiecki and Raymo, 2005; Railsback et al., 2015) (Fig. 3). To facilitate comparison with other proxy and model reconstructions we use the recent substage nomenclature, as recommended by Railsback et al. (2015), as well as the decimal event notation because it distinguishes additional $\delta^{18}O_b$ isotopic events reflecting the orbital-scale variability within MIS 13.

3.2. Pollen and biomarker analyses

A total of 265 levels from Site U1385 were sampled for pollen analysis every 2–4 cm and prepared following the protocol established at the UMR EPOC (Oceanic and Continental Environments and Paleoenvironments), University of Bordeaux (http://www.epoc.u-bordeaux.fr/) described by Oliveira (2017). Pollen samples were processed using an optimized protocol for marine samples including coarse-sieving (150 μm mesh), successive treatments with cold HCl and cold HF, micro-sieving (10 μm mesh) and slide mounting in glycerol. A mean of 23 pollen morphotypes (17–30) and 113 (93–220) pollen grains excluding *Pinus*, *Cedrus*, aquatics plants (*Sparganium-Typha*, *Myriophylllum*-type, *Nuphar* and *Polygonum persicaria*-type) and Pteridophyta spores were counted per sample to provide a reliable image of the vegetation community and its floristic diversity (McAndrews and King, 1976). Pollen zones were identified visually from the pollen diagram shown in Fig. 2 and confirmed using the constrained cluster analysis based squared Euclidian dissimilarity (CONISS) implemented in PSIMPOLL (Bennett, 2009). The Mediterranean forest pollen percentage (MF) record includes all temperate tree and shrub taxa excluding *Pinus, Cedrus* and Cupressaceae (*Acer, Alnus, Betula, Carpinus, Castanea, Corylus, Fagus, Fraxinus excelsior*-type, *Hedera helix, Ilex, Juglans, Ligustrum*-type, *Myrica, Populus, Pterocarya, Quercus deciduous*-type, *Salix, Tilia, Ulmus* and *Vitis*) and Mediterranean sclerophylls (*Quercus evergreen*-type, *Quercus suber*-type, *Cistus, Olea, Pistacia* and *Phillyrea*). Following experimental studies showing that arboreal pollen percentages (AP%) reflect past tree cover patterns (e.g., Williams and Jackson, 2003), we interpret the Site U1385 MF record as an indicator of the SW Iberian tree fraction.

The alkenone-based sea surface temperature ($U^{k'}_{37}$-SST) profile is a higher resolution version of the record of Rodrigues et al. (2017), in which the sampling interval was increased up to 2–4 cm (312 new samples). Alkenones were quantified from the total lipid extraction (TLE) by removing 2g of sediment through sonication with dichloromethane and hydrolysed with 6% potassium hydroxide in methanol. After derivatization with bis(-trimethylsilyl)trifluoroacetamide, the TLE was identified using Bruker Mass spectrometer detector and quantified with a Varian Gas chromatograph Model 3800 equipped with septum programmable injector and a flame ionization detector with a CPSIL-5 CB column. Hydrogen was used as gas carrier (2.5 ml/min). The quantification of di and tri-unsaturated alkenones of 37 carbons was performed following the methods described in Rodrigues et al. (2017). SST estimation was based on Müller et al. (1998) equation. The estimated analytical precision of this method is about 0.5 °C.

3.3. Model experiments

The climate model experiments were performed with the three-dimensional Earth system model of intermediate complexity LOVECLIM, including coupled dynamic atmosphere (ECBilt), sea-ice-ocean (CLIO) and terrestrial biosphere (VECODE) components, while the oceanic carbon cycle (LOCH) and the ice-sheets (AGISM) are prescribed to their present-day configuration. VECODE (Vegetation COntinuous DEscription model) is a reduced-form dynamical global vegetation model that simulates two basic plant functional types, trees and grass. Their area concentration in a land grid cell (tree fraction or grass fraction) is governed by empirical relationships in view of the annual precipitation and the positive degree-days (Brovkin et al., 1997). For each land grid cell, the tree and grass fractions match the vegetation fraction and the rest corresponds to the desert fraction. LOVECLIM has been successfully used in multiple climate studies involving a significant range of distinct boundary conditions of the past, present and future, and at global and regional scales. An extensive description of the model is provided in Goosse et al. (2010).

To study the effects of the NH ice-sheets on the tree fraction and climate over SW Iberia, we performed two sensitivity experiments

Fig. 2. Percentage pollen diagram of selected morphotypes and ecological groups from Site U1385 plotted against depth. Ecological groups include Mediterranean forest (MF, Mediterranean sclerophylls and all temperate trees and shrub taxa, excluding *Pinus*, *Cedrus* and Cupressaceae; Mediterranean sclerophylls: *Quercus evergreen*-type, *Quercus suber*-type, *Cistus, Olea, Pistacia* and *Phillyrea*; semi-desert plants: *Artemisia*, Chenopodiaceae, *Ephedra*-type; and ubiquist plants: all herbaceous taxa excluding Ericaceae and semi-desert plants. On the right of the diagram are represented the pollen zones and the dendrogram showing the results of the cluster analysis. Pollen zones are labeled as following: Site U1385 - MIS - number of the pollen zone. Shaded green areas indicate MF major expansions (MF ~>35%) within Oeiras, the terrestrial counterpart of MIS 13 in SW Iberia. (For interpretation of the references to color in this figure legend, the reader is referred to the Web version of this article.)

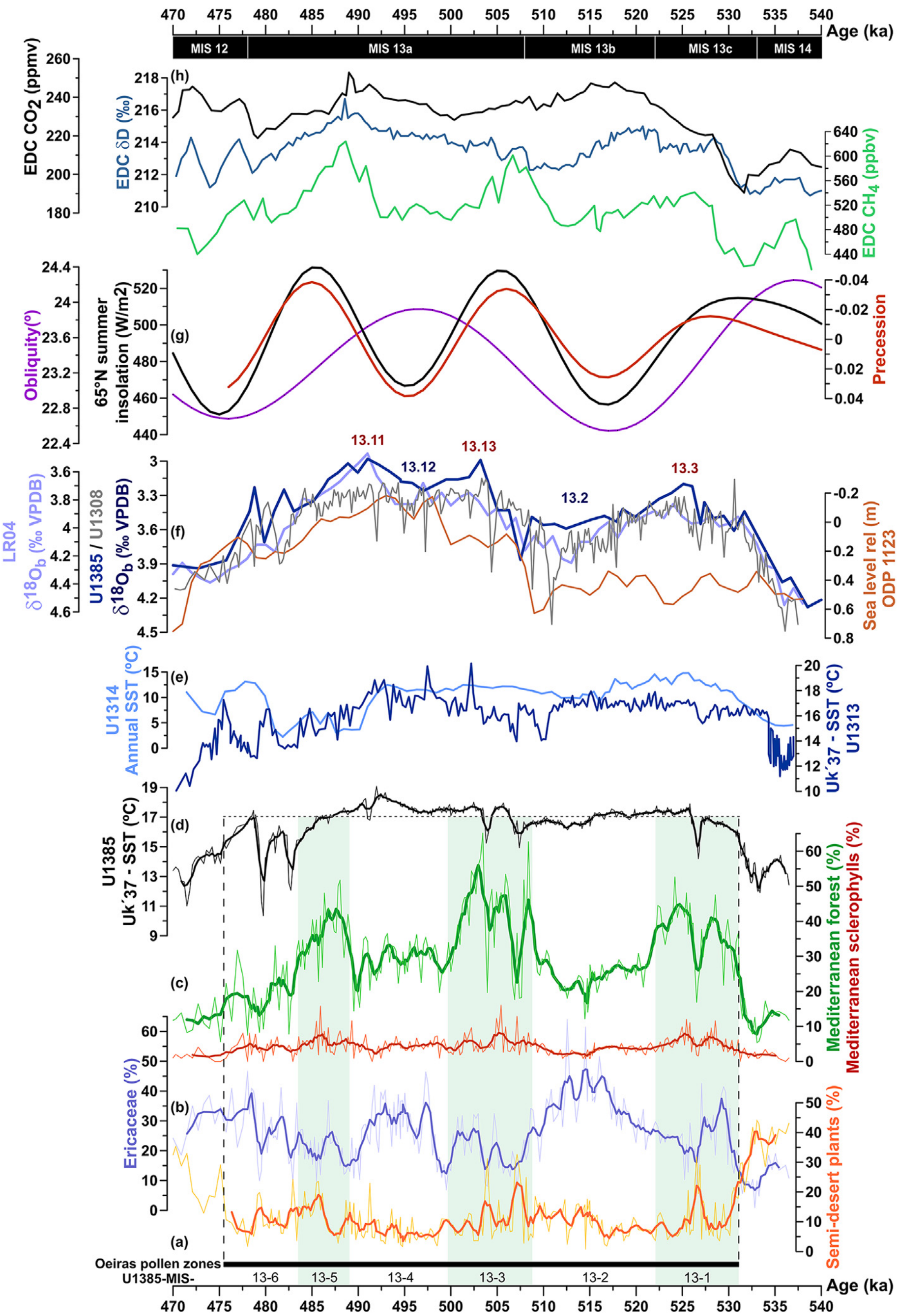

Fig. 3. MIS 13 vegetation and climatic changes at Site U1385. From bottom to top: Percentages of selected pollen taxa or group of taxa: (a) semi-desert plants (orange), (b) Ericaceae (heathlands) (blue), (c) Mediterranean sclerophylls (red) and Mediterranean forest (MF) (green); (d) Site U1385 $U^{k'}_{37}$-SST (black). Bold lines represent 5-point moving averages from a-d. (e) Site U1313 $U^{k'}_{37}$-SST (Naafs et al., 2012) (dark blue) and Site U1314 MAT-mean annual SST (Alonso-Garcia et al., 2011) (light blue); (f) $\delta^{18}O_b$ records of Sites U1385 (Hodell et al., 2015) (dark blue), U1308 (Hodell et al., 2008) (grey) and LR04 (Lisiecki and Raymo, 2005) (light blue) with MIS 13 marine isotopic events. $\delta^{18}O$ seawater-based sea-level relative changes (Elderfield et al., 2012) (orange); (g) 65°N summer insolation (black), obliquity (purple) and precession (red) parameters (Berger, 1978). (h) EPICA Dome C temperature anomaly (Jouzel et al., 2007) (blue), CO_2 (Lüthi et al., 2008) (black) and CH_4 concentrations (Loulergue et al., 2008) (green). Green bands mark the MF major expansions during Oeiras interglacial based on the zonation of the pollen diagram (Fig. 2) at the bottom. MIS substages following Railsback et al. (2015) are shown at the top. (For interpretation of the references to color in this figure legend, the reader is referred to the Web version of this article.)

from Yin et al. (2008). One is “no ice” experiment, where insolation and GHG of the MIS 13.13 climate optimum, assumed to be at 506 ka when NH summer occurred at perihelion, are used, but the present-day ice-sheets are prescribed. Another is “ice” experiment, where additional ice-sheets are prescribed over North America and Eurasia. The calculation and configuration of MIS 13.13 ice-sheets are presented in detail in Yin et al. (2008). Estimations of ice-sheet volume are based on different individual $\delta^{18}O_b$ profiles and global stacks and their locations determined by extrapolating the information available for the Last Glacial Maximum (LGM). The calculation leads to a North America ice-sheet of 7.3 × 10^6 km^3 centered at 90°W, 69°N, and an Eurasian ice-sheet of 3.7 × 10^6 km^3 centered at 50°E, 63°N. The present-day Greenland ice-sheet is of 2.9 × 10^6 km^3. The effect of the two additional ice-sheets is assessed by comparing the results of the “ice” and “no ice” experiments (Figs. 4 and 5).

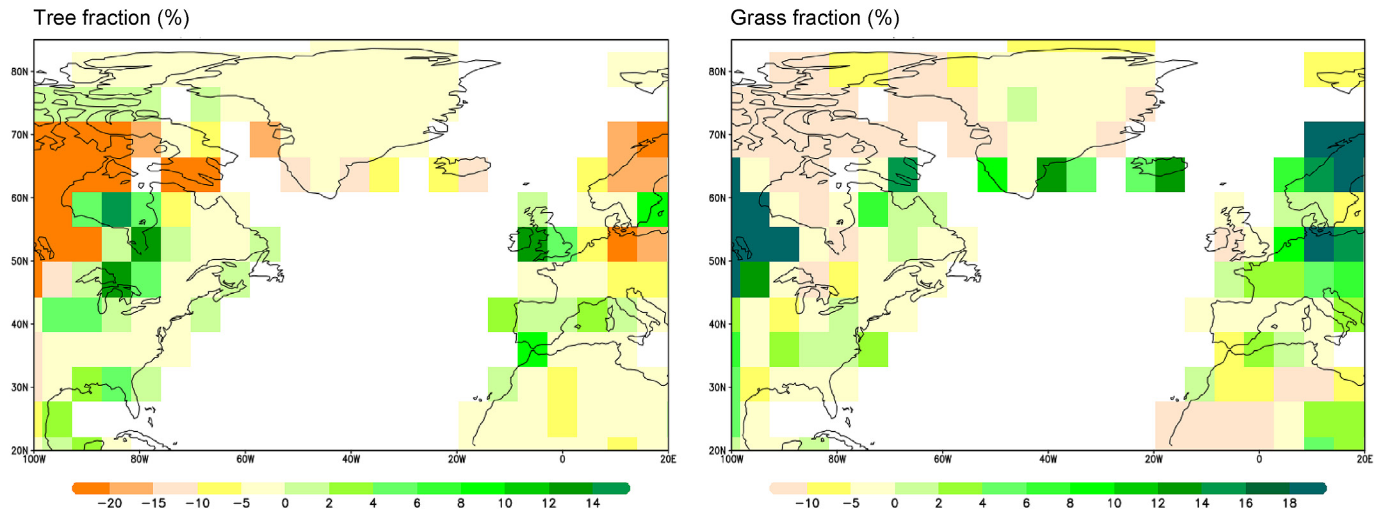

Fig. 4. Difference in the tree and grass fraction (%) (left and right panels, respectively) at 506 ka between the experiment "ice" (MIS 13.13 North American and Eurasian ice-sheets) and the experiment "no ice" (present-day ice-sheets). Grid plot using the land-sea configuration in LOVECLIM.

4. Results and discussion

4.1. MIS 13 southern European vegetation and climate

Constrained hierarchical cluster analysis allowed the pollen diagram to be divided into eight pollen zones (Figs. 2 and 3). Glacial sections of MIS 14 and MIS 12 are recorded as open vegetation phases (U1385-14-1 and -12-1, respectively) dominated by semi-desert vegetation and grassland (Poaceae and *Taraxacum*-type) with *Pinus*, indicating prevailing cold and arid conditions (Figs. 2 and 3). The SW Iberian counterpart of MIS 13, named Oeiras, lasts from 531 to 480 ka and comprises six pollen zones (U1385-13-1 to −6) characterized by MF values mostly above 20% (Figs. 2 and 3), which is in line with the threshold defined in marine records for representing interglacial forest development (Sánchez Goñi et al., 2016, 2018, 2019; Tzedakis et al., 2004; Roucoux et al., 2006; Oliveira et al., 2016, 2017).

This 51-kyr long and floristically diverse forest stage is characterized by a complex of three pronounced forest expansions and intervening intervals of more open vegetation (Figs. 2 and 3). The major forest phases, U1385-13-1, -13-3 and -13-5 encompassing MIS 13.3, 13.13 and 13.11, respectively, are essentially characterized by a well-developed MF dominated by deciduous *Quercus* (MF ~35–65%), the occurrence of various cool-temperate taxa such as *Alnus*, *Carpinus*, *Corylus*, *Fagus*, *Fraxinus excelsior*, *Hedera* and *Ulmus*, and a weak representation of thermophilous and summer drought-adapted Mediterranean sclerophylls (mean 5.5%) (Figs. 2 and 3). Based on present-day climatic requirements, these vegetation types reflect a cool-temperate and particularly humid climate regime characterized by a reduced seasonal contrast (e.g., Polunin and Walters, 1985; Blanco Castro et al., 1997). The prominent development of Ericaceae (mean 22%) further supports our interpretation as this family thrives under a temperate and moist climate with cool winters and low rainfall seasonality (Polunin and Walters, 1985; Loidi et al., 2007). In contrast to the other SW Iberian interglacials of the last 800 kyr (Sánchez Goñi et al., 2016, 2018, 2019; Tzedakis et al., 2004; Roucoux et al., 2006; Oliveira et al., 2016; IODP Site 1385 unpublished data), the maximum extent of the MF reflecting increased warmth and humidity within MIS 13, is not recorded during the earliest phase of the interglacial but during the second forest phase (-13-3, ~509–501 ka), associated with MIS 13.13. During the other phases of forest expansions (-13-1, 531–522 ka; and -13-5, ~489–483 ka), the MF extent reached a similar magnitude, however, the reduced development of heathlands during the younger and shorter forest phase suggests relatively cooler and less moist conditions. Phases of open forest, U1385-13-2, -13-4 and -13-6, associated with MIS 13.2, 13.12 and the MIS 13.13-MIS 12 transition, respectively, are represented by MF decreases to moderate values (MF ~20–35%) episodically crossing the 20% threshold (Figs. 2 and 3), indicating a shift to cooler and drier conditions but most often not below the bioclimatic thresholds required to sustain forest development.

Similar to Site U1385, Tenaghi Philippon and Lake Ohrid pollen sequences show an extensive forest period marked by three major expansions of oak, suggesting overall warmth and/or moisture availability (Tzedakis et al., 2006; Wagner et al., 2019). Conversely, high humidity levels and mild winters are clearly documented by the Italian records of Vallo di Diano and Ceprano, in southern and central Italy respectively, through the strong expansion of mixed mesothermic forest and the significant presence of waterlogging-tolerant trees (e.g., *Alnus* and *Ulmus*) and moisture-demanding taxa (*Hedera*) (Russo Ermolli et al., 2015; Margari et al., 2018). A notably wet climate for MIS 13 in Europe is also supported by small-vertebrate fossil remains in Spain (Blain et al., 2012), and by eastern European loess-paleosol sequences (Markovic et al., 2009; Fitzsimmons et al., 2012).

The U1385 $U^{k'}_{37}$-SST profile shows a long period of relatively stable conditions, but cooler than present-day, with SSTs around ~17 °C on average. Stadial conditions of MIS 13.2 are only marked by a slight SST decrease of less than ~1 °C, close to the analytical uncertainty of 0.5 °C, while no cooling is recorded during MIS 13.12. The warmest SSTs, ~18.5 °C, are also recorded during MIS 13a but during the phase of more open vegetation U1385-13-4 (Fig. 3). The complex climatic structure of Oeiras at orbital-scale with three distinct forest peaks is, therefore, not paralleled by the $U^{k'}_{37}$ -SST record. Noticeably, at millennial-scale, few abrupt coolings centered ~526.7, 507.4, 503.8, 482.7 and 479.8 ka are synchronously detected on land (Fig. 3). The atypical late position of the MIS 13 thermal optimum emerges as a consistent characteristic of this interglacial, being recorded in the Mediterranean Sea and in the North Atlantic ocean (e.g., Voelker et al., 2010; Rodrigues et al., 2011; Naafs et al., 2012; Marino et al., 2014; Candy et al., 2015; Martin-Garcia et al., 2015; Marino et al., 2018), with the exception of IODP Site U1314 and ODP Site 983 (Alonso-Garcia et al., 2011;

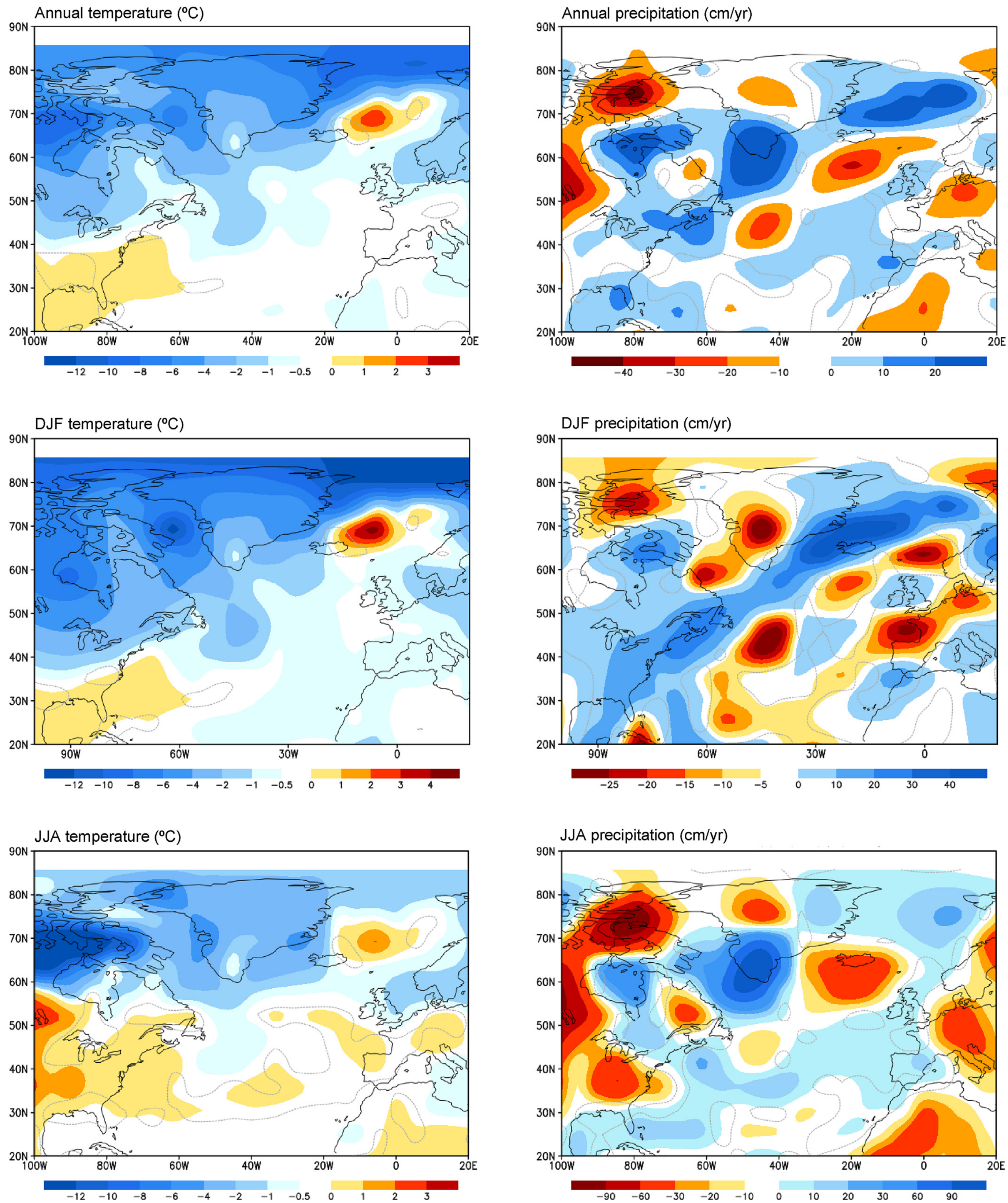

Fig. 5. Difference in the annual mean, winter (DJF) and summer (JJA) surface air temperature (°C) and precipitation (cm/year) (left and right panels, respectively) at 506 ka between the experiment "ice" (MIS 13.13 North American and Eurasian ice-sheets) and the experiment "no ice" (present-day ice-sheets). The color shading indicates the regions for which the simulated anomalies are significantly different at the 95% confidence level based on a *t*-test while the contour lines limit the changes that are not significant. (For interpretation of the references to color in this figure legend, the reader is referred to the Web version of this article.)

Barker et al., 2019) in the subpolar gyre (Fig. 1), as well as the muted SST changes during MIS 13.2 (e.g., Voelker et al., 2010; Rodrigues et al., 2011; Naafs et al., 2012; Cortina et al., 2016) (Fig. 3). This oceanic optimum appears mostly associated with the reconstructed global sea-level maximum/ice volume minimum (Bintanja et al., 2005; Lisiecki and Raymo, 2005; Elderfield et al., 2012; Spratt and Lisiecki, 2016), as well as to the Antarctic temperature and CO_2 concentration maxima (Jouzel et al., 2007; Lüthi et al., 2008; Bereiter et al., 2015) occurring during the late MIS 13a (Fig. 3). In contrast, the atmospheric CH_4 concentration (Loulergue et al., 2008) shows the same internal three-peak structure as the pollen-based vegetation record from Site U1385. However, subevent MIS 13.11 is slightly stronger than 13.13 (Fig. 3), which further underlines the degree of complexity in the regional and global expression of the climate optimum during late MIS 13.

4.2. The complex land-sea-ice interactions throughout MIS 13

The close correspondence between insolation changes and the major shifts between forest expansion and more open vegetation conditions during MIS 13 reflects the dominant influence of this forcing on the SW Iberian vegetation (Fig. 3). The impact of precession is also clearly noted in the development of the Mediterranean sclerophylls, although tenuous, during the intervals of precession minima and in the expansion of heathlands under precession maxima (Fig. 3). This vegetation response is consistent with the influence of precession on the seasonal contrast over the Mediterranean region, south of 40°N, (Ruddiman and McIntyre, 1984), and its imprint on the SW Iberian vegetation across the middle-to late Pleistocene and Holocene (e.g., Oliveira et al., 2017; Sánchez Goñi et al., 2018, 2019; Gomes et al., 2020).

Although insolation minima during MIS 13 are among the strongest of the last 800 kyr (Berger, 1978), the forest did not collapse as expected. We suggest that these limited forest reductions may be linked to persisting warm STTs off SW Iberia and associated relatively subdued ice volume changes during MIS 13, as observed in the $\delta^{18}O_b$ records and sea-level reconstructions (Lisiecki and Raymo, 2005) (Fig. 3). Moreover, during the MIS 13b substage, the $\delta^{18}O_b$ values barely exceeded 3.5‰ (Fig. 3), a critical ice volume threshold for the cooling event amplification associated with ice-sheet dynamic processes (McManus et al., 1999), and related forest contractions in Iberia (Desprat et al., 2009; Margari et al., 2010; Oliveira et al., 2016, 2017). However, no millennial variability that could have driven episodical forest shrinkage is observed in the North Atlantic SST and ice-rafted debris records during this stadial (e.g., Alonso-Garcia et al., 2011; Hodell et al., 2008; Barker et al., 2019). The interval of limited forest extent, between 501 and 489 ka (U1385-13-4), occurs during the warmest SSTs over the Iberian margin and the North Atlantic and concurred with obliquity maxima counterbalancing the effect of precession-driven ice growth during mid-MIS 13a (Fig. 3). Model simulations focusing on the climatic effects of the high-versus-low obliquity during the similar precession forcing of MIS 13.12 and 13.2 (495 and 516 ka time slices) (Fig. 3) have shown that the MIS 13.12 obliquity maximum causes a warming over the NH high latitudes that may have limited ice-sheet growth and delayed the glacial inception process (Rachmayani et al., 2016). As the atmospheric circulation in the mid-latitudes is mostly determined by the latitudinal thermal contrast over the North Atlantic (e.g., Brayshaw et al., 2011), this hypothesis is supported by our multiproxy reconstruction showing that a reduced meridional thermal gradient (due to warm mid-to-high latitudes) may have led to a weakening and southward deviation of the westerlies that sustained SW Iberian forest development (Fig. 3). This influence of the westerlies in the studied region would imply a reduction in the northward transport of moisture that is necessary for the build-up of NH ice-sheets, which may have contributed to preclude glacial inception and to the particular long duration of MIS 13.

4.3. How does MIS 13 stand out from other interglacials within the last 800 kyr?

Although there is still an ongoing debate about the global and regional imprint of the MBE in the interglacials within the last 800 kyr, recent data compilations and model simulations provide clear evidence for the distinct weak/cool character of MIS 13 regardless of spatial heterogeneity (e.g., Yin and Berger, 2012; Lang and Wolff, 2011; Candy and McClymont, 2013; Past Interglacials Working Group of PAGES, 2016; Rodrigues et al., 2017; Barth et al., 2018; Candy and Alonso-Garcia, 2018). So far, interglacial intensity has been mostly estimated in terms of thermal regime, ice volume/sea-level and GHG concentrations with little attention paid to precipitation patterns. However, in regions with landscapes and ecosystems highly susceptible to hydrological changes, such as the Mediterranean, it is crucial to consider precipitation changes. Given both present-day and past dependence of the SW Iberian forest on winter rainfall (e.g., Gouveia et al., 2008; Oliveira et al., 2018), the long pollen record from Site U1385 allows us to evaluate the intensity of the MIS 13 Oeiras interglacial, in terms of forest expansion and precipitation regime, in the context of other middle-to late Pleistocene interglacials. Here, following recent work (Past Interglacials Working Group of PAGES, 2016; Oliveira et al., 2018), we estimate interglacial intensity based on the maximum values achieved in the interval comprising the major development of MF and Mediterranean sclerophylls (Table 2) as it reflects the optimal expression of Mediterranean climate conditions (Polunin and Walters, 1985).

The comparison of SW Iberian interglacials shows that the optimum forest development differs substantially between interglacials (MF ~44–78%) although there is no expression of the MBE as the tree cover maximum was higher, on average, during the pre-MBE than during the post-MBE interglacials (Table 2). Most importantly, it reveals that MIS 13 does not stand out as a weak interglacial over the western Mediterranean (Table 2). MIS 13.13 displays the major forest expansion after MIS 17.3 and a maximum similar to MIS 5.5, one of the strongest interglacials globally (MIS 13.13: 65.2%, MIS 5.5: 68.7%, MIS 17.3: 77.7% - Table 2). Moreover, among all interglacials, the vegetation composition of MIS 13 at the forest optimum emerges as unique, being characterized by the lowest abundances of Mediterranean sclerophylls and the strongest development of heathlands (Table 2). From a climatic point of view, this comparison shows that in SW Iberia, MIS 13 differs from the other interglacials for its cool-temperate climate regime marked by high levels of humidity and the lowest seasonal contrast between the cool-wet winters and warm-dry summers typical of this region. In contrast, although noticed as one of the strongest, the MIS 13 forest expansion at the Tenaghi Philippon and Lake Ohrid sites does not appear as conspicuously more prominent (Table 2). Both pollen sequences rather exhibit similar interglacial forest expansions throughout the last 650 kyr (Tzedakis et al., 2006; Wagner et al., 2019). The marked differences between Site U1385 and these pollen sequences lend support to the idea that the forest ecological requirements may vary between southern European regions. In European sequences located above 40°N, forest development was likely mainly limited by temperature, suggesting that similar interglacial AP% reflect similar atmospheric warmth, while in the southerly regions the primary limiting factor was moisture availability (Desprat et al., 2017; Sánchez Goñi et al., 2018). In addition, the continental Tenaghi Philippon and Lake Ohrid sites are under the influence of both Mediterranean and continental climate (e.g.,

Table 2
Maximum values for the peak interglacials of the past 800 kyr at Site U1385 records (this work; Tzedakis et al., 2004; Roucoux et al., 2006; Sánchez Goñi et al., 2018, 2019; Hodell et al., 2015; Rodrigues et al., 2017) and other terrestrial (Tzedakis et al., 2006; Wagner et al., 2019) and global reconstructions referred to in this study (Lisiecki and Raymo, 2005; Bintanja et al., 2005; Lüthi et al., 2008; Spratt and Lisiecki, 2016) along with insolation (Berger, 1978). Values for 13.13 are shown when the sub-events of 13.1 are distinguished. *Site U1385 (Tenaghi Philippon and Lake Ohrid) pollen data for MIS 7.5 (7.1) and 15.5 (15.1), corresponding to the isotopic events where the maxima arboreal pollen (AP) % was achieved.

		Post- MBE				Pre- MBE			
	MIS isotopic events	5.5	7.5*	9.5	11.3	13.1/13.13	15.5*	17.3	19.3
Site U1385	Time comprising the maximal expansion of MF and Mediterranean sclerophylls (ka BP)	127.1–128.4	239.7–240.9	327.6.-328.8	408.3–409.6	502.2–503.5	620.4–619.1	695.2–694.1	784–785.5
	MF maximum (average) %	68.7 (64.5)	43.9 (43)	55.9 (51.6)	43.8 (40)	65.2 (55.7)	62.1 (53.3)	77.7 (72.2)	45.5 (38.8)
	Mediterranean sclerophylls maximum (average) %	20.6 (17.6)	16.2 (10.8)	23.8 (19.6)	17 (11.9)	9.6 (4.8)	31.3 (21.3)	12.4 (9.4)	23.6 (15.2)
	Ericaceae maximum (average) %	9.8 (8.1)	9.2 (6.9)	19.8 (14.4)	22.9 (17.5)	32.4 (25.4)	9.7 (6.3)	8.8 (5.2)	14.9 (11.9)
	Maximum Uk'$_{37}$-SST (°C)	20.8	19.6	20.7	18.8	19.0	20.0	20.4	21.1
	Benthic $\delta^{18}O_b$ (‰)	2.4	2.76	2.58	2.70	3.09	2.87	3.02	2.86
Tenaghi Philippon	AP maximum %	96	95.8	95.5	99.5	95.8	96.9	82.2	83.3
Lake Ohrid	AP maximum %	92.8	89.2	91.5	81.2	93.5	92.4	65.7	83
Antarctic EDC ice core	CO_2 (ppmv)	285.8	280.2	298.6	285.6	252.8	259.7	243.6	269.4
Insolation	65°N insolation at summer solstice (W/m^2)	548	529	542	523	530	545	543	532
LR04 stack	Benthic $\delta^{18}O_b$ (‰)	3.10	3.44	3.19	3.11	3.68	3.49	3.50	3.48
Modeled global sea level	Global sea level relative to present (m)	0	−19	−0.5	0	−29	−26	−22	−20
Sea level stack	Sea level (m NN)	−1	−9	−2	16	−11	−9	−10	−6

Xoplaki et al., 2003; Popovska and Bonacci, 2007), conditions likely to determine the observed regional variability in southern European vegetation (Desprat et al., 2017). Other long continental records across the NH also contradict the view of a MIS 13 widespread weakness, even if for some of the terrestrial proxies the environmental/climatic relation is yet not clear, such as for the biosilica content from the Siberian Lake Baikal and the Si/Ti of the Russian Lake El'gygytgyn (Past Interglacials Working Group of PAGES, 2016 and references therein). Remarkably, MIS 13 is typically the strongest interglacial in the long sequences from the East Asian monsoon region (e.g., Xifeng loess section, China: Guo et al., 2009), and is among the most intense in the African monsoon records (e.g., eastern Mediterranean ODP Sites 968 and 968: Ziegler et al., 2010; Konijnendijk et al., 2014; Past Interglacials Working Group of PAGES, 2016).

The observed cool-temperate climate regime marked by enhanced precipitation in SW Iberia is associated with one of the coolest interglacial SSTs of the last 800 kyr, as recorded by North Atlantic records (e.g., Lang and Wolff, 2011; Past Interglacials Working Group of PAGES, 2016) including Site U1385 (Table 2; Rodrigues et al., 2017). Interestingly, shorter Iberian margin records report for MIS 13 similar cooler conditions along with particularly intense continental input and marine productivity (MIS 9–15, MD03-2699: Rodrigues et al., 2011; MIS 10–16, U1385: Maiorano et al., 2015). We propose that pronounced continental input, likely fostered by our pollen-inferred high levels of precipitation, may have contributed to enhance the marine productivity during MIS 13 by increasing the river flow of nutrient-rich waters into the Iberian margin as observed for the Holocene (Rodrigues et al., 2009). This unusual high productivity during MIS 13 has been related to worldwide-scale changes in the global ocean carbon reservoir as expressed by the most prominent peak of benthic $\delta^{13}C_b$ in individual and global datasets of the last 800 kyr (e.g., Wang et al., 2004; Lisiecki, 2014; Barth et al., 2018; Rodrigues et al., 2017). The most common causes of the outstanding $\delta^{13}C_b$ excursion during MIS 13 involve (i) enhanced precipitation leading to higher incursion of silica-enriched waters (Wang et al., 2004); (ii) stronger North Atlantic Deep Water production (Raymo et al., 1997; Ziegler et al., 2010); and (iii) increased continental biomass while the levels of CO_2 and ocean export productivity remained similar to other pre-MBE interglacials (Raymo et al., 1990; Yin and Guo, 2008; Barth et al., 2018). Barth et al. (2018) argue that the $\delta^{13}C_b$ excursion is due to an increase in terrestrial biomass in the NH allowing for a larger ^{13}C-depleted storage and resulting from the combined effect of weak MIS 14 glaciation and strong monsoonal precipitation over MIS 13. Our study and other long European pollen sequences (Tzedakis et al., 2006; Wagner et al., 2019) reconstructing particularly high forest development during MIS 13 (Table 2) give support to this hypothesis and emphasizes the need to consider other important forested areas of the NH besides the monsoon regions.

4.4. Is ice-sheet forcing the key to understand the forest optimum of MIS 13 in SW Iberia?

The MIS 13 pollen record from Site U1385 provides one of the clearest evidences for the apparent lack of relationship between CO_2 and the Mediterranean forest extent given that high MF development occurred under particularly low interglacial CO_2 concentrations (Fig. 3, Table 2). This observation is in line with model experiments demonstrating that interglacial CO_2 changes have a minor effect on the global tree fraction change and particularly over the northern tropical-subtropical regions (Yin and Berger, 2012), including SW Iberia (Oliveira et al., 2018). Conversely, insolation is found to be the primary driver of the simulated vegetation change due to the strong impact of precession on the precipitation regimes of these regions (Yin and Berger, 2012; Oliveira et al., 2018). Although these model experiments reproduce the well-documented impact of precession on the Mediterranean vegetation (e.g., Tzedakis, 2007; Sánchez Goñi et al., 2018), insolation alone is insufficient to explain the different magnitude of the terrestrial interglacials in SW Iberia over the past 800 kyr (Table 2). However, these simulations are only forced by GHG and insolation whilst ice-sheets were not taken into account (Yin and Berger, 2012; Oliveira et al., 2018). The absence of ice-sheets and related feedbacks in the simulations has been proposed as the main cause for discrepancies between SW Iberia's pollen-based and modeled interglacial tree fraction optimum in MIS 19 (Oliveira et al., 2018). Recent snapshot simulations comparing the response of the carbon cycle to the different climate configurations of the pre- and post-MBE interglacials show that ice-sheets play a crucial role on setting the regional vegetation cover (Bouttes et al., 2018). In particular, the agreement between models and reconstructions of southern European vegetation is improved when the different interglacial ice-sheets are included in the modeling experiments. Despite deep-sea temperature overprinting on $\delta^{18}O_b$ (e.g., Skinner and Shackleton, 2005), MIS 13.13 consistently emerges as one of the most glaciated interglacials of the past 800 kyr in the LR04 stack (Lisiecki and Raymo, 2005) and individual $\delta^{18}O_b$ reconstructions (e.g., Site U1308: Hodell et al., 2008) including that of Site U1385 (Fig. 3, Table 2). Modeled global sea-level (Bintanja et al., 2005) and sea-level stack (Spratt and Lisiecki, 2016, and references therein) support a relatively low highstand (Table 2). Spahni et al. (2005) suggested that the intermediate warmth of MIS 13 limited the shrinkage of the NH ice-sheets leading to its southernmost interglacial extension of the last 650 kyr. The apparent exception to this pattern is based on the high pollen content at ODP Site 646 (Labrador Sea) during MIS 13 interpreted as a result of a much more reduced Greenland ice-sheet than on other interglacials besides MIS 11 (de Vernal and Hillaire-Marcel, 2008). Nonetheless, it has been argued that this potential loss of the Greenland ice-sheet during MIS 13 did not lead to an overall low ice extent compared to other interglacials (Past Interglacials Working Group of PAGES, 2016) and may be the result of persistent warm conditions over MIS 15-13 due to the unusual weak glacial climate of MIS 14 (Lang and Wolff, 2011).

To investigate the potential impact of the relatively large NH ice-sheets of MIS 13 on SW Iberia, we performed LOVECLIM experiments designed to isolate the response of the regional vegetation and climate to the ice-sheet forcing presumed to exist at the interglacial peak (MIS 13.13 time-slice at 506 ka). Fig. 4 shows that the addition of the North America and Eurasian ice-sheets leads to a significant increase in the Iberian tree fraction, particularly over the southern part of the Peninsula (up to 10%), revealing that these ice-sheets indeed contribute to increase the forest optimum of MIS 13. As in the vegetation component of LOVECLIM (VECODE), the tree fraction is a function of annual temperature and precipitation (Brovkin et al., 1997), the analysis of these parameters clearly shows that the SW Iberian tree fraction increase is driven by higher annual precipitation as there is no change in the surface temperature over this region with the inclusion of ice-sheet forcing (Figs. 4 and 5). This dominant influence of precipitation on the modeled tree fraction is consistent with our expectations based on the terrestrial–marine climate records of Site U1385, which consider regional hydroclimate as the primary determinant of MIS 13 vegetation patterns. Moreover, the model simulations show that the presence of ice-sheets in North America and Eurasia causes an intensification of the winter precipitation over SW Iberia and a reduction in the typical Mediterranean summer dryness, as shown by the rainfall increase during summertime (Fig. 5). These model results successfully show that including ice-sheet forcing favors the climate conditions necessary for the three key vegetation features observed at the MIS 13 optimum (Figs. 2 and 3, Table 2), namely: (i) wetter summers and reduced seasonality restricting the expansion of Mediterranean sclerophylls, (ii) sustained humidity year-round and cool temperatures explaining strong development of heathlands, and (iii) a temperate environment with high moisture availability enabling the occurrence of diverse temperate and summer drought-intolerant trees along with strong expansion of deciduous oaks (Polunin and Walters, 1985; Blanco Castro et al., 1997; Loidi et al., 2007). Therefore, we suggest that the regional signature of MIS 13 over southern Iberia is explained by the amplification of the insolation forcing by the relatively high ice volume of this interglacial.

This supplementary forcing may have played a key role in changing the large-scale atmospheric circulation, which ultimately resulted in a temperate climate characterized by enhanced humidity and weak seasonality over the studied region. The influence of the same ice-sheets on the East Asian climate was reported in previous work using both LOVECLIM and Hadley Centre Coupled Model (HadCM3) (Yin et al., 2008, 2009; Muri et al., 2013). These model experiments show that the topography of the Eurasian ice-sheet can induce an atmospheric wave train across the Eurasian continent propagating southeastward that leads to exceptionally strong EASM precipitation and higher tree fraction. Interestingly, in our model simulations a similar large-scale wave train is found in precipitation (Fig. 5) and pressure fields across the North Atlantic and Europe. This wave train is initiated from the North American ice-sheet and propagates southeastward. It is most pronounced in the winter precipitation with alternating dry and wet anomalies elongating in northwest-southeast direction with a wet anomaly over SW Iberia. In our study, the wave pattern is induced by the North American ice-sheet topography as shown by a sensitivity experiment where only the Laurentide ice-sheet is imposed (Sundaram et al., 2012). It corresponds to the barotropic model results of Grose and Hoskins (1979) and Hoskins and Karoly (1981). Actually, many climate simulations have shown that the large Laurentide ice-sheet over the last glacial could alter the large-scale atmosphere circulations over the Atlantic (e.g., Löfverström et al., 2014). Although only a small Laurentide ice-sheet is used in our modeling experiments, the results show that it is large enough (more than 2000 m high) to alter the Atlantic atmosphere circulation.

In addition, the large remnant ice-sheets of MIS 13 could lead to a more southerly position of the atmospheric circulation systems than during the other interglacials, including the parallel displacement of the Hadley and Ferrel cells and associated mid-latitude westerlies controlling the SW Iberian winter hydroclimate (e.g., Lionello et al., 2006). Indeed, a southward position of the North Atlantic jet stream and the deviation of the storm tracks transporting moisture into SW Iberia has been reported for the last glacial period (e.g., Laîné et al., 2009; Beghin et al., 2015), with significant increase of precipitation over Iberia (Ludwig et al., 2016), although probably to a much larger extent due to the glacial climate context (higher ice volume). These inferred shifts in the atmospheric circulation during MIS 13 would also imply a southward position of the Intertropical Convergence Zone (ITCZ) and associated subtropical subsidence influencing the SW Iberian summer dryness (e.g., Lionello et al., 2006). A more southerly position of the North Atlantic Subtropical High would decrease the influence of high-pressure systems over southern Iberia leading to reduced summer dryness, and, therefore, to higher annual moisture availability and muted seasonality as indicated by the pollen-based vegetation of Site U1385 and model results (Figs. 3–5). This conceptual model is consistent with previous work linking SW European vegetation and hydroclimate changes for the past 800 kyr to the prevalence of low or mid latitudinal forcing depending on the ITCZ position, which in turn is strongly influenced by ice volume conditions (Tzedakis et al., 2009).

Considering the importance of ice-sheet forcing to explain the SW Iberian vegetation and climate of MIS 13.13, a similar climate-driven forest optimum would be expected for the other pre-MBE interglacials characterized by relatively high ice volume baseline conditions and high insolation (Table 2). Interestingly, while MIS 15.5 and 17.3 are marked by high forest development, MIS 19.3 exhibits a rather low forest extent of just 45% (Table 2). We speculate that the different configuration of NH ice-sheets during MIS

19.3 (larger Eurasian ice-sheet development) may have caused a reduced penetration of the winter storm tracks into the Iberian region with subsequent reduced forest expansion, as suggested by Oliveira et al. (2018). Long and accurate ice-sheet reconstructions and new interglacial data-model comparisons are definitively needed to explore the impact of changes in extent and configuration of the ice-sheets on regional precipitation, a key factor controlling the amplitude of MF development and vegetation composition.

5. Conclusions

MIS 13 regional expression and underlying forcing mechanisms are investigated for the first time in the western Mediterranean through new multiproxy reconstructions from IODP Site U1385 and its comparison with climate-model experiments. Our findings demonstrate the importance of combining insolation and ice-sheet forcing to explain the regional vegetation and climate imprint of MIS 13. The major findings are summarized hereunder.

1. The strong Mediterranean forest development and vegetation composition during MIS 13 reveals a cool-temperate climate with relatively high levels of humidity and reduced seasonal contrast over the SW Iberian region.
2. This warm stage is marked by three insolation-driven forest expansions interrupted by muted contractions despite strong precession forcing. While terrestrial and marine climate profiles agree on the cool character of MIS 13, a land-sea decoupling is noted through the interglacial, being particularly evident on the asynchronous time of forest and ocean surface temperature optima during MIS 13a. The moderate forest extent and associated influence of the westerlies in this region during mid-MIS 13a indicates a reduction in the transport of moisture nourishing the NH ice-sheets that may have prevented the end of MIS 13 at this time (~495 ka).
3. MIS 13 stands out from the other SW Iberian interglacials of the last 800 kyr for its large optimum forest development of weak Mediterranean character. This finding highlights that increased land biomass during MIS 13 was not limited to the monsoon regions, supporting the view that a larger terrestrial carbon storage may have contributed to the unusual carbon isotope excursion recorded in the different ocean basins.
4. The model-data comparison reveals that the dominant effect of MIS 13 insolation forcing on the regional vegetation and precipitation regime in SW Iberia is amplified by the relatively large extent of the ice-sheets in high northern latitudes at the interglacial peak (MIS 13.13). In qualitative agreement with the pollen-based evidence, model results show that ice-sheet forcing triggers an increase in the SW Iberian tree fraction along with both intensified winter and summer rainfall. The topography of the North American ice-sheet induces an atmospheric wave train propagating southeastward leading to a wetter situation in SW Iberia, visible in both summer and winter seasons, albeit more pronounced in the latter. The relatively large interglacial ice-sheets during MIS 13 could also lead to a southward shift of the North Atlantic jet stream and the ITCZ which consequently increase the large-scale winter and summer precipitation in SW Iberia, and therefore, higher forest cover with reduced Mediterranean sclerophyllous vegetation.

Author statement

D.O.: Conceptualization, Formal analysis, Visualization, Writing - Original Draft; S.D., M.S.G., Q.Y.: Conceptualization, Resources; Q.Y., Q.S., T.R., J.O.G., M.A.-G., A.V.: Formal analysis; F.N.: Funding acquisition; S.D., Q.Y., T.R., F.N., R.M.T, Q.S., J.O.G., M. A.-G., A.V., F.A., M.S.G.: Writing - Review & Editing.

Declaration of competing interest

The authors declare that they have no known competing financial interests or personal relationships that could have appeared to influence the work reported in this paper.

Acknowledgments

Financial support was provided by the Portuguese Foundation for Science and Technology (FCT) through the project CLIMHOL (PTDC/AAC-CLI/100157/2008), ULTImATum (IF/01489/2015), SAICT-45-2017-02 projects (WARM WORLDS: 29897 and HOLMODRIVE: 29029), CCMAR FCT Research Unit - project UIDB/04326/2020, D. Oliveira's contract (CEECIND/02208/2017), F. Naughton's contract (IF/01489/2015), T. Rodrigues's contract (WarmWorld- PTDC/CTA-GEO/29897/2017), Voelker's contract (IF/01500/2014), and Warm-Clim, a LEFE-INSU IMAGO project. D. Oliveira acknowledges the fundng provided by the L'Oréal Portugal Medal of Honour for Women in Science 2018 from L'Oréal, FCT and UNESCO. M. Alonso-Garcia acknowledges funding from FCT through the CINNAMOW project (PTDC/MAR-PRO/3396/2014) and the Spanish Ministry of Science through the grant RTI2018-099489-B-I00. Q. Yin is a Research Associate of the Belgian National Fund for Scientific Research (FRS-FNRS). Computational resources have been provided by the supercomputing facilities of the Université catholique de Louvain (CISM/UCL) and the Consortium des Equipements de Calcul Intensif en Fédération Wallonie Bruxelles (CECI) funded by FRS-FNRS. We would like to thank the scientists and technicians of IODP Expedition 339, the Bremen Core Repository, L. Devaux for technical assistance, V. Hanquiez for drawing Fig. 1., and two anonymous reviewers for their constructive comments.

References

Alonso-Garcia, M., Sierro, F.J., Kucera, M., Flores, J.A., Cacho, I., Andersen, N., 2011. Ocean circulation, ice sheet growth and interhemispheric coupling of millennial climate variability during the mid-Pleistocene (ca 800–400 ka). Quat. Sci. Rev. 30, 3234–3247. https://doi.org/10.1016/j.quascirev.2011.08.005.

Barker, S., Knorr, G., Conn, S., Lordsmith, S., Newman, D., Thornalley, D., 2019. Early interglacial legacy of deglacial climate instability. Paleoceanogr Paleoclimatol 34, 1455–1475. https://doi.org/10.1029/2019PA003661.

Barth, A.M., Clark, P.U., Bill, N.S., He, F., Pisias, N.G., 2018. Climate evolution across the mid-Brunhes transition. Clim. Past 14, 2071–2087. https://doi.org/10.5194/cp-14-2071-2018.

Bassinot, F.C., Labeyrie, L.D., Vincent, E., Quidelleur, X., Shackleton, N.J., Lancelot, Y., 1994. The astronomical theory of climate and the age of the Brunhes-Matuyama magnetic reversal. Earth Planet Sci. Lett. 126, 91–108.

Beghin, P., Charbit, S., Kageyama, M., Combourieu-Nebout, N., Hatté, C., Dumas, C., Peterschmitt, J.-Y., 2015. What drives LGM precipitation over the western Mediterranean? A study focused on the Iberian Peninsula and northern Morocco. Clim. Dynam. 46, 2611–2631. https://doi.org/10.1007/s00382-015-2720-0.

Bennett, K.D., 2009. Documentation for Psimpoll 4.27 and Pscomb 1.03. C Programs for Plotting and Analyzing Pollen Data: the ^{14}Chrono Centre, Archaeology and Palaeoecology.

Bereiter, B., Eggleston, S., Schmitt, J., Nehrbass-Ahles, C., Stocker, T.F., Fischer, H., Kipfstuhl, S., Chappellaz, J., 2015. Revision of the EPICA Dome C CO_2 record from 800 to 600 kyr before present. Geophys. Res. Lett. 42, 542–549. https://doi.org/10.1002/2014GL061957.

Berger, A., 1978. Long-Term variations of daily insolation and Quaternary climatic changes. J. Atmos. Sci. 35, 2362–2367.

Bintanja, R., van de Wal, R.S.W., Oerlemans, J., 2005. Modelled atmospheric temperatures and global sea levels over the past million years. Nature 437, 125–128. https://doi.org/10.1038/nature03975.

Blain, H.-A., Cuenca-Bescos, G., Lozano-Fernandez, I., Lopez-Garcia, J.M., Olle, A., Rosell, J., Rodriguez, J., 2012. Investigating the mid-Brunhes event in the Spanish terrestrial sequence. Geology 40, 1051–1054. https://doi.org/10.1130/G33427.1.

Blanco Castro, E., Casado González, M.A., Costa Tenorio, M., Escribano Bombín, R., García Antón, M., Génova Fuster, M., Gómez Manzaneque, F., Moreno Sáiz, J.C., Morla Juaristi, C., Regato Pajares, P., Sáiz Ollero, H., 1997. Los Bosques Ibéricos: Una Interpretación Geobotánica. Editorial Planeta, Barcelona, p. 572.

Bouttes, N., Swingedouw, D., Roche, D.M., Sánchez Goñi, M.F., Crosta, X., 2018. Response of the carbon cycle in an intermediate complexity model to the different climate configurations of the last nine interglacials. Clim. Past 14, 239–253. https://doi.org/10.5194/cp-14-239-2018.

Brayshaw, D.J., Rambeau, C.M.C., Smith, S.J., 2011. Changes in Mediterranean climate during the Holocene: insights from global and regional climate modelling. Holocene 21, 15–31. https://doi.org/10.1177/0959683610377528.

Brovkin, V., Ganopolski, A., Svirezhev, Y., 1997. A continuous climate-vegetation classification for use in climate-biosphere studies. Ecol. Model. 101, 251–261. https://doi.org/10.1016/S0304-3800(97)00049-5.

Candy, I., Alonso-Garcia, M., 2018. A 1 Ma sea surface temperature record from the North Atlantic and its implications for the early human occupation of Britain. Quat. Res. 90, 406–417. https://doi.org/10.1017/qua.2018.62.

Candy, I., Mcclymont, E.L., 2013. Interglacial intensity in the north atlantic over the last 800000 years: investigating the complexity of the mid-Brunhes event. J. Quat. Sci. 28, 343–348. https://doi.org/10.1002/jqs.2632.

Candy, I., Schreve, D., White, T.S., 2015. MIS 13-12 in Britain and the north atlantic: understanding the palaeoclimatic context of the earliest acheulean. J. Quat. Sci. 30, 593–609. https://doi.org/10.1002/jqs.2816.

Cortina, A., Grimalt, J.O., Martrat, B., Rigual-Hernández, A., Sierro, F.J., Flores, J.A., 2016. Anomalous SST warming during MIS 13 in the gulf of lions (northwestern Mediterranean Sea). Org. Geochem. 92, 16–23. https://doi.org/10.1016/j.orggeochem.2015.12.004.

de Vernal, A., Hillaire-Marcel, C., 2008. Natural variability of Greenland climate, vegetation, and ice volume during the past million years. Science 320, 1622–1625. https://doi.org/10.1126/science.1153929.

Desprat, S., Oliveira, D., Naughton, F., Sánchez Goñi, M.F., 2017. L'étude du pollen des séquences sédimentaires marines pour la compréhension du climat: L'exemple des périodes chaudes passées. Quaternaire 28, 259–269. https://doi.org/10.4000/quaternaire.8102.

Desprat, S., Sánchez Goñi, M.F., McManus, J.F., Duprat, J., Cortijo, E., 2009. Millennial-scale climatic variability between 340000 and 270000 years ago in SW Europe: evidence from a NW Iberian margin pollen sequence. Clim. Past 5, 53–72. https://doi.org/10.5194/cp-5-53-2009.

Di Rita, F., Sottili, G., 2019. Pollen analysis and tephrochronology of a MIS 13 lacustrine succession from eastern sabatini volcanic district (Rignano Flaminio, central Italy). Quat. Sci. Rev. 204, 78–93. https://doi.org/10.1016/j.quascirev.2018.11.027.

Elderfield, H., Ferretti, P., Greaves, M., Crowhurst, S., McCave, N., Hodell, D., Piotrowski, A.M., 2012. Evolution of ocean temperature and ice volume through the Mid- Pleistocene climate transition. Science 377, 704–709. https://doi.org/10.1126/science.1221294.

Fitzsimmons, K.E., Marković, S.B., Hambach, U., 2012. Pleistocene environmental dynamics recorded in the loess of the middle and lower Danube basin. Quat. Sci. Rev. 41, 104–118. https://doi.org/10.1016/j.quascirev.2012.03.002.

Fiúza, A.F.G., 1984. Hidrologia e Dinâmica das Águas Costeiras de Portugal. Univ. de Lisboa, Lisbon, p. 294. Ph.D. thesis.

Gomes, S., Fletcher, W.J., Rodrigues, T., Stone, A., Abrantes, F., Naughton, F., 2020. Time-transgressive Holocene maximum of temperate and Mediterranean forest development across the Iberian Peninsula reflects orbital forcing. Palaeogeogr. Palaeoclimatol. Palaeoecol. 550, 109739. https://doi.org/10.1016/j.palaeo.2020.109739.

Goosse, H., Brovkin, V., Fichefet, T., Haarsma, R., Huybrechts, P., Jongma, J., Mouchet, A., Selten, F., Barriat, P.-Y., Campin, J.-M., Deleersnijder, E., Driesschaert, E., Goelzer, H., Janssens, I., Loutre, M.-F., Maqueda, M.A., Opsteegh, T., Mathieu, P.-P., Munhoven, G., Pettersson, E.J., Renssen, H., Roche, D.M., Schaeffer, M., Tartinville, B., Timmermann, A., Weber, S.L., 2010. Description of the Earth system model of intermediate complexity LOVECLIM version 1.2. Geosci. Model Dev. (GMD) 3, 603–633.

Gouveia, C., Trigo, R.M., DaCamara, C.C., Libonati, R., Pereira, J.M.C., 2008. the North atlantic oscillation and European vegetation dynamics. Int. J. Climatol. 28, 1835–1847.

Grose, W.L., Hoskins, B.J., 1979. On the influence of orography on large-scale Atmospheric flow. J. Atmos. Sci. 36, 223–234.

Guo, Z.T., Berger, A., Yin, Q.Z., Qin, L., 2009. Strong asymmetry of hemispheric climates during MIS-13 inferred from correlating China loess and Antarctica ice records. Clim. Past 5, 21–31. https://doi.org/10.5194/cp-5-21-2009.

Hodell, D., Lourens, L., Crowhurst, S., Konijnendijk, T., Tjallingii, R., Jimenez-Espejo, F., Skinner, L., Tzedakis, P.C., 2015. A reference time scale for site U1385 (Shackleton site) on the SW iberian margin. Global Planet. Change 1385, 49–64. https://doi.org/10.1016/j.gloplacha.2015.07.002.

Hodell, D.A., Channell, J.E.T., Curtis, J.H., Romero, O.E., Röhl, U., 2008. Onset of "Hudson strait" Heinrich events in the eastern North Atlantic at the end of the middle Pleistocene transition (~640 ka)? Paleoceanography 23, 1–16. https://doi.org/10.1029/2008PA001591.

Hoskins, B.J., Karoly, D.J., 1981. The steady linear response of a spherical atmosphere to thermal and orographic forcing. J. Atmos. Sci. 38, 1179–1196.

Jansen, J.H.F., Kuijpers, A., Troelstra, S.R., 1986. A mid-Brunhes climatic event: long-term changes in global atmospheric and ocean circulation. Science 232, 619–622.

Jouzel, J., Masson-Delmotte, V., Cattani, O., Dreyfus, G., Falourd, S., Hoffmann, G., Minster, B., Nouet, J., Barnola, J.M., Chappellaz, J., Fischer, H., Gallet, J.C., Johnsen, S., Leuenberger, M., Loulergue, L., Luethi, D., Oerter, H., Parrenin, F., Raisbeck, G., Raynaud, D., Schilt, A., Schwander, J., Selmo, E., Souchez, R., Spahni, R., Stauffer, B., Steffensen, J.P., Stenni, B., Stocker, T.F., Tison, J.L., Werner, M., Wolff, E.W., 2007. Orbital and millennial Antarctic climate variability over the past 800,000 years. Science 317, 793–796. https://doi.org/10.1126/science.1141038.

Konijnendijk, T.Y.M., Ziegler, M., Lourens, L.J., 2014. Chronological constraints on Pleistocene sapropel depositions from high-resolution geochemical records of ODP Sites 967 and 968. Newsl. Stratigr. 47 (3), 263–282. https://doi.org/10.1127/0078-0421/2014/0047.

Laîné, A., Kageyama, M., Salas-Mélia, D., Voldoire, A., Rivière, G., Ramstein, G., Planton, S., Tyteca, S., Peterschmitt, J.Y., 2009. Northern hemisphere storm tracks during the last glacial maximum in the PMIP2 ocean atmosphere coupled models: energetic study, seasonal cycle, precipitation. Clim. Dynam. 32, 593–614.

Lang, N., Wolff, E.W., 2011. Interglacial and glacial variability from the last 800 ka in marine, ice and terrestrial archives. Clim. Past 7, 361–380. https://doi.org/10.5194/cp-7-361-2011.

Lionello, P., Malanotte-Rizzoli, P., Boscolo, R., Alpert, P., Artale, V., Li, L., Luterbacher, J., May, W., Trigo, R., Tsimplis, M., Ulbrich, U., Xoplaki, E., 2006. The Mediterranean climate: an overview of the main characteristics and issues. Dev. Earth Environ. Sci. 4, 1–26. https://doi.org/10.1016/S1571-9197(06)80003-0.

Lisiecki, L.E., 2014. Atlantic overturning responses to obliquity and precession over the last 3 Myr. Paleoceanography 29, 71–86.

Lisiecki, L.E., Raymo, M.E., 2005. A Pliocene–Pleistocene stack of 57 globally-distributed benthic $\delta^{18}O$ records. Paleoceanography 20, PA1003. https://doi.org/10.1029/2004PA001071.

Löfverström, M., Caballero, R., Nilsson, J., Kleman, J., 2014. Evolution of the large-scale atmospheric circulation in response to changing ice sheets over the last glacial cycle. Clim. Past 10, 1453–1471. https://doi.org/10.5194/cp-10-1453-2014.

Loidi, J., Biurrun, I., Campos, J.A., Garcıa-Mijangos, I., Herrera, M., 2007. A survey of heath vegetation of the Iberian Peninsula and Northern Morocco: a biogeographical and bioclimatic approach. Phytocoenologia 37, 341–370.

Loulergue, L., Schilt, A., Spahni, R., Masson-Delmotte, V., Blunier, T., Lemieux, B., Barnola, J.-M., Raynaud, D., Stocker, T.F., Chappellaz, J., 2008. Orbital and millennial-scale features of atmospheric CH_4 over the past 800,000 years. Nature 453, 383–386. https://doi.org/10.1038/nature06950.

Lu, H., Yin, Q., Jia, J., Xia, D., Gao, F., Lyu, A., Ma, Y., Yang, F., 2020. Possible link of an exceptionally strong East Asian summer monsoon to a La Niña-like condition during the interglacial MIS-13. Quat. Sci. Rev. 227 https://doi.org/10.1016/j.quascirev.2019.106048.

Ludwig, P., Schaffernicht, E.J., Shao, Y., Pinto, J.G., 2016. Regional atmospheric circulation over Europe during the last glacial maximum and its links to precipitation. J. Geophys. Res. Atmos. 121, 2130–2145. https://doi.org/10.1002/2015JD024444.

Lüthi, D., Le Floch, M., Bereiter, B., Blunier, T., Barnola, J.-M., Siegenthaler, U., Raynaud, D., Jouzel, J., Fischer, H., Kawamura, K., Stocker, T.F., 2008. High-resolution carbon dioxide concentration record 650,000-800,000 years before present. Nature 453, 379–382. https://doi.org/10.1038/nature06949.

Maiorano, P., Marino, M., Balestra, B., Flores, J.-A., Hodell, D.A., Rodrigues, T., 2015. Coccolithophore variability from the Shackleton site (IODP site U1385) through MIS 16-10. Global Planet. Change 133, 35–48. https://doi.org/10.1016/j.gloplacha.2015.07.009.

Margari, V., Roucoux, K., Magri, D., Manzi, G., Tzedakis, P.C., 2018. The MIS 13 interglacial at Ceprano, Italy, in the context of Middle Pleistocene vegetation changes in southern Europe. Quat. Sci. Rev. 199, 144–158. https://doi.org/10.1016/j.quascirev.2018.09.016.

Margari, V., Skinner, L.C., Tzedakis, P.C., Ganopolski, A., Vautravers, M., Shackleton, N.J., 2010. The nature of millennial-scale climate variability during the past two glacial periods. Nat. Geosci. 3, 127–131.

Marino, M., Girone, A., Maiorano, P., Di Renzo, R., Piscitelli, A., Flores, J.A., 2018. Calcareous plankton and the mid-Brunhes climate variability in the Alboran Sea (ODP Site 977). Palaeogeogr. Palaeoclimatol. Palaeoecol. 508, 91–106. https://doi.org/10.1016/j.palaeo.2018.07.023.

Marino, M., Maiorano, P., Tarantino, F., Voelker, A., Capotondi, L., Girone, A., Lirer, F., Flores, J.A., Naafs, B.D.A., 2014. Coccolithophores as proxy of seawater changes at orbital-to-millennial scale during middle Pleistocene Marine Isotope Stages 14-9 in North Atlantic core MD01-2446. Paleoceanography 29, 518–532. https://doi.org/10.1002/2013PA002574.

Marković, S.B., Hambach, U., Catto, N., Jovanovic, M., Buggle, B., Machalett, B., Zöller, L., Glaser, B., Frechen, M., 2009. Middle and late Pleistocene loess sequences at Batajnica, vojvodina, Serbia. Quat. Int. 198, 255–266.

Martin-Garcia, G.M., Alonso-Garcia, M., Sierro, F.J., Hodell, D.A., Flores, J.A., 2015. Severe cooling episodes at the onset of deglaciations on the Southwestern Iberian margin from MIS 21 to 13 (IODP site U1385). Global Planet. Change 135, 159–169.

McAndrews, J.H., King, J., 1976. Pollen of the north American quaternary: the top twenty. Geosci. Man 15, 41–49.

McManus, J.F., Oppo, D.W., Cullen, J.L., 1999. A 0.5-million-year record of millennial-scale climate variability in the north atlantic. Science 283, 971–974.

Morales-Molino, C., Devaux, L., Georget, M., Hanquiez, V., Sánchez Goñi, M.F., 2020. Modern pollen representation of the vegetation of the Tagus basin (central iberian Peninsula). Rev. Palaeobot. Palynol. 276, 104193. https://doi.org/10.1016/j.revpalbo.2020.104193.

Müller, P.J., Kirst, G., Ruhland, G., Von Storch, I., Rosell-Melé, A., 1998. Calibration of the alkenone paleotemperature index $U^{K'}_{37}$- based on core-tops from the eastern South Atlantic and the global ocean (60°N-60°S). Geochem. Cosmochim. Acta 62, 1757–1772.

Muri, H., Berger, A., Yin, Q., Karami, M.P., Barriat, P.Y., 2013. The climate of the MIS-13 interglacial according to HadCM3. J. Clim. 26, 9696–9712. https://doi.org/10.1175/JCLI-D-12-00520.1.

Muri, H., Berger, A., Yin, Q., Voldoire, A., Mélia, D.S.Y., Sundaram, S., 2012. SST and ice sheet impacts on the MIS-13 climate. Clim. Dynam. 39, 1739–1761. https://doi.org/10.1007/s00382-011-1216-9.

Naafs, B.D.A., Hefter, J., Acton, G., Haug, G.H., Martinez-Garcia, A., Pancost, R.D., Stein, R., 2012. Strengthening of North American dust sources during the late Pliocene (2.7 Ma). Earth Planet Sci. Lett. 317, 8–19. https://doi.org/10.1016/j.epsl.2011.11.026.

Naughton, F., Sánchez Goñi, M.F., Desprat, S., Turon, J.L., Duprat, J., Malaizé, B., Joli, C., Cortijo, E., Drago, T., Freitas, M.C., 2007. Present-day and past (last 25 000 years) marine pollen signal off western Iberia. Mar. Micropaleontol. 62, 91–114. https://doi.org/10.1016/j.marmicro.2006.07.006.

Oliveira, D., 2017. Understanding Warm Periods within and after the Mid Pleistocene Transition (MIS 31 and 11) in the Iberian Peninsula. Bordeaux University, France, p. 292. PhD Thesis. http://www.theses.fr/2017BORD0598.

Oliveira, D., Desprat, S., Rodrigues, T., Naughton, F., Hodell, D., Trigo, R., Rufino, M., Lopes, C., Abrantes, F., Sánchez Goñi, M.F., 2016. The complexity of millennial-scale variability in southwestern Europe during MIS 11. Quat. Res. 86, 373–387. https://doi.org/10.1016/j.yqres.2016.09.002.

Oliveira, D., Desprat, S., Yin, Q., Naughton, F., Trigo, R., Rodrigues, T., Abrantes, F., Sánchez Goñi, M.F., 2018. Unraveling the forcings controlling the vegetation and climate of the best orbital analogues for the present interglacial in SW Europe. Clim. Dynam. 51, 667–686. .org/10.1007/s00382-017-3948-7.

Oliveira, D., Sánchez Goñi, M.F., Naughton, F., Polanco-Martínez, J.M., Jimenez-Espejo, F.J., Grimalt, J.O., Martrat, B., Voelker, A.H.L., Trigo, R., Hodell, D., Abrantes, F., Desprat, S., 2017. Unexpected weak seasonal climate in the western Mediterranean region during MIS 31, a high-insolation forced interglacial. Quat. Sci. Rev. 161, 1–17. https://doi.org/10.1016/j.quascirev.2017.02.013.

Past Interglacials Working Group of PAGES, 2016. Interglacials of the last 800,000 years. Rev. Geophys. 54 https://doi.org/10.1002/2015RG000482.

Polunin, O., Walters, M., 1985. A Guide to the Vegetation of Britain and Europe. Oxford University Press, New York 238pp.

Popovska, C., Bonacci, O., 2007. Basic data on the hydrology of lakes Ohrid and Prespa. Hydrol. Process. 21 (5), 658–664.

Rachmayani, R., Prange, M., Schulz, M., 2016. Intra-interglacial climate variability: model simulations of marine isotope stages 1, 5, 11, 13, and 15. Clim. Past 12, 677–695. https://doi.org/10.5194/cp-12-677-2016.

Railsback, L.B., Gibbard, P.L., Head, M.J., Voarintsoa, N.R.G., Toucanne, S., 2015. An optimized scheme of lettered marine isotope substages for the last 1.0 million years, and the climatostratigraphic nature of isotope stages and substages. Quat. Sci. Rev. 111, 94–106. https://doi.org/10.1016/j.quascirev.2015.01.012.

Raymo, M.E., Oppo, D.W., Curry, W., 1997. The mid-Pleistocene climate transition: a deep sea carbon isotopic perspective. Paleoceanography 12, 546–559.

Raymon, M.E., Ruddiman, W.F., Shackleton, N.J., Oppo, D.W., 1990. Evolution of atlantic–Pacific $\delta^{13}C$ gradients over the last 2.5 My. Earth Planet Sci. Lett. 97, 353–368.

Rodrigues, T., Alonso-García, M., Hodell, D.A., Rufino, M., Naughton, F., Grimalt, J.O., Voelker, A.H.L., Abrantes, F., 2017. A 1-Ma record of sea surface temperature and extreme cooling events in the North Atlantic: a perspective from the Iberian Margin. Quat. Sci. Rev. 172, 118–130.

Rodrigues, T., Grimalt, J.O., Abrantes, F., Flores, J.A., Lebreiro, S., 2009. Holocene interdependences of changes in sea surface temperature, productivity and fluvial inputs in the Iberian continental shelf (Tagus mud patch). G-cubed 10 (7). https://doi.org/10.1029/2008GC002367.

Rodrigues, T., Voelker, A.H.L., Grimalt, J.O., Abrantes, F., Naughton, F., 2011. Iberian Margin sea surface temperature during MIS 15 to 9 (580–300 ka): glacial suborbital variability versus interglacial stability. Paleoceanography 26. https://doi.org/10.1029/2010PA001927. PA1204.

Rossignol-Strick, M., Paterne, M., Bassinot, F.C., Emeis, K.-C., De Lange, G.J., 1998. An unusual mid-Pleistocene monsoon period over Africa and Asia. Nature 392, 269–272.

Roucoux, K.H., Tzedakis, P.C., de Abreu, L., Shackleton, N.J., 2006. Climate and vegetation changes 180,000 to 345,000 years ago recorded in a deep-sea core off Portugal. Earth Planet Sci. Lett. 249, 307–325. https://doi.org/10.1016/j.epsl.2006.07.005.

Ruddiman, W.F., McIntyre, A., 1984. Ice-age thermal response and climatic role of the surface Atlantic Ocean, 40°N to 63°N. Geol. Soc. Am. Bull. 95, 381–396.

Russo Ermolli, E., Di Donato, V., Martín-Fernandez, J.A., Orain, R., Lebreton, V., Piovesan, G., 2015. Vegetation patterns in the Southern Apennines (Italy) during MIS 13: deciphering pollen variability along a NW-SE transect. Rev. Palaeobot. Palynol. 218, 167–183.

Sánchez Goñi, M.F., Desprat, S., Fletcher, W.J., Morales-Molino, C., Naughton, F., Oliveira, D., Urrego, D.H., Zorzi, C., 2018. Pollen from the deep-sea: a breakthrough in the Mystery of the ice ages. Front. Plant Sci. 9 https://doi.org/10.3389/fpls.2018.00038.

Sánchez Goñi, M.F., Ferretti, P., Polanco-Martínez, J.M., Rodrigues, T., Alonso-García, M., Rodríguez-Tovar, F.J., Dorador, J., Desprat, S., 2019. Pronounced northward shift of the westerlies during MIS 17 leading to the strong 100-kyr ice age cycles. Earth Planet Sci. Lett. 511, 117–129. https://doi.org/10.1016/j.epsl.2019.01.032.

Sánchez Goñi, M.F., Rodrigues, T., Hodell, D.A., Polanco-Martínez, J.M., Alonso-García, M., Hernández-Almeida, I., Desprat, S., Ferretti, P., 2016. Tropically-driven climate shifts in southwestern Europe during MIS 19, a low eccentricity interglacial. Earth Planet Sci. Lett. 448, 81–93. https://doi.org/10.1016/j.epsl.2016.05.018.

Skinner, L.C., Shackleton, N.J., 2005. An Atlantic lead over Pacific deep-water change across Termination I: implications for the application of the marine isotope stage stratigraphy. Quat. Sci. Rev. 24, 571–580. https://doi.org/10.1016/j.quascirev.2004.11.008.

Spahni, R., Chappellaz, J., Stocker, T.F., Loulergue, L., Hausammann, G., Kawamura, K., Fluckiger, J., Schwander, J., Raynaud, D., Masson-Delmotte, V., Jouzel, J., 2005. Atmospheric methane and nitrous oxide of the late Pleistocene from antarctic ice cores. Science 310, 1317–1321.

Spratt, R.M., Lisiecki, L.E., 2016. A Late Pleistocene sea level stack. Clim. Past 12, 1079–1092. https://doi.org/10.5194/cp-12-1079-2016.

Sundaram, S., Yin, Q.Z., Berger, A., Muri, H., 2012. Impact of ice sheet induced North Atlantic oscillation on East Asian summer monsoon during an interglacial 500,000 years ago. Clim. Dynam. 39, 1093–1105. https://doi.org/10.1007/s00382-011-1213-z.

Teles-Machado, A., Peliz, A., McWilliams, J.C., Couvelard, X., Ambar, I., 2016. Circulation on the northwestern iberian margin: vertical structure and seasonality of the alongshore flows. Prog. Oceanogr. 140, 134–153. doi:10.1016/j.pocean.2015.05.021.

Trigo, R.M., Pozo- Vázquez, D., Osborn, T.J., Castro-Díez, Y., Gamiz-Fortis, S., Esteban-Parra, M.J., 2004. North Atlantic Oscillation influence on precipitation, river flow and water resources in the Iberian Peninsula. Int. J. Climatol. 24, 925–944. https://doi.org/10.1002/joc.1048.

Tzedakis, P.C., Roucoux, K.H., de Abreu, L., Shackleton, N.J., 2004. The duration of forest stages in southern Europe and interglacial climate variability. Science 306, 2231–2235. https://doi.org/10.1126/science.1102398.

Tzedakis, P.C., 2007. Seven ambiguities in the Mediterranean palaeoenvironmental narrative. Quat. Sci. Rev. 26, 2042–2066. https://doi.org/10.1016/j.quascirev.2007.03.014.

Tzedakis, P.C., Hooghiemstra, H., Pälike, H., 2006. The last 1.35 million years at Tenaghi Philippon: revised chronostratigraphy and long-term vegetation trends. Quat. Sci. Rev. 25, 3416–3430. https://doi.org/10.1016/j.quascirev.2006.09.002.

Tzedakis, P.C., Pälike, H., Roucoux, K.H., de Abreu, L., 2009. Atmospheric methane, southern European vegetation and low-mid latitude links on orbital and millennial timescales. Earth Planet Sci. Lett. 277, 307–317. https://doi.org/10.1016/j.epsl.2008.10.027.

Voelker, A.H.L., Rodrigues, T., Billups, K., Oppo, D., McManus, J., Stein, R., Hefter, J., Grimalt, J.O., 2010. Variations in mid-latitude North Atlantic surface water properties during the mid-Brunhes (MIS 9–14) and their implications for the thermohaline circulation. Clim. Past 6, 531–552. https://doi.org/10.5194/cp-6-531-2010.

Wagner, B., Vogel, H., Francke, A., Friedrich, T., Donders, T., Lacey, J.H., Leng, M.J., Regattieri, E., Sadori, L., Wilke, T., Zanchetta, G., Albrecht, C., Bertini, A., Combourieu-Nebout, N., Cvetkoska, A., Giaccio, B., Grazhdani, A., Hauffe, T., Holtvoeth, J., Joannin, S., Jovanovska, E., Just, J., Kouli, K., Kousis, I., Koutsodendris, A., Krastel, S., Lagos, M., Leicher, N., Levkov, Z., Lindhorst, K., Masi, A., Melles, M., Mercuri, A.M., Nomade, S., Nowaczyk, N., Panagiotopoulos, K., Peyron, O., Reed, J.M., Sagnotti, L., Sinopoli, G., Stelbrink, B., Sulpizio, R., Timmermann, A., Tofilovska, S., Torri, P., Wagner-Cremer, F., Wonik, T., Zhang, X., 2019. Mediterranean winter rainfall in phase with African monsoons during the past 1.36 million years. Nature 573, 256–260. https://doi.org/10.1038/s41586-019-1529-0.

Wang, P., Tian, J., Cheng, X., Liu, C., Xu, J., 2004. Major Pleistocene stages in a carbon perspective: the South China Sea record and its global comparison. Paleoceanography 19, PA4005. https://doi.org/10.1029/2003PA000991.

Williams, J.W., Jackson, S.T., 2003. Palynological and AVHRR observations of modern vegetational gradients in eastern North America. Holocene 13, 485–497. https://doi.org/10.1191/0959683603hl613rp.

Xoplaki, E., González-Rouco, J.F., Luterbacher, J., Wanner, H., 2003. Mediterranean summer air temperature variability and its connection to the large-scale atmospheric circulation and SSTs. Clim. Dynam. 20 (7–8), 723–739.

Yin, Q.Z., Berger, A., 2010. Insolation and CO_2 contribution to the interglacial climate before and after the Mid-Brunhes Event. Nat. Geosci. 3 (4), 243–246.

Yin, Q.Z., Berger, A., 2012. Individual contribution of insolation and CO_2 to the interglacial climates of the past 800,000 years. Clim. Dynam. 38, 709–724. https://doi.org/10.1007/s00382-011-1013-5.

Yin, Q.Z., Berger, A., Crucifix, M., 2009. Individual and combined effects of ice sheets and precession on MIS-13 climate. Clim. Past 5, 229–243. https://doi.org/10.5194/cp-5-229-2009.

Yin, Q.Z., Berger, A., Driesschaert, E., Goosse, H., Loutre, M.F., Crucifix, M., 2008. The Eurasian ice sheet reinforces the East Asian summer monsoon during the interglacial 500 000 years ago. Clim. Past 4, 79–90. https://doi.org/10.5194/cp-4-79-2008.

Yin, Q.Z., Guo, Z.T., 2008. Strong summer monsoon during the cool MIS-13. Clim. Past 4, 29–34. https://doi.org/10.5194/cp-4-29-2008.

Ziegler, M., Lourens, L.J., Tuenter, E., Reichart, G.J., 2010. High Arabian Sea productivity conditions during MIS 13-odd monsoon event or intensified overturning circulation at the end of the Mid-Pleistocene transition? Clim. Past 6, 63–76. https://doi.org/10.5194/cp-6-63-2010.